Ag Nanoparticle-Mediated Raman Scattering of 4-Aminobenzenethiol on a Pt Substrate

Kwan Kim,*,† Hyang Bong Lee,† Jae Keun Yoon,† Dongha Shin,† and Kuan Soo Shin*,‡

Department of Chemistry, Seoul National University, Seoul 151-742, Korea, and Department of Chemistry, Soongsil University, Seoul 156-743, Korea

Received: June 1, 2010; Revised Manuscript Received: July 13, 2010

Raman scattering measurements were conducted for 4-aminobenzenethiol (4-ABT) monolayers assembled on a macroscopically smooth Pt substrate. At the beginning, no Raman peak was detected for 4-ABT on Pt, but upon attaching Ag nanoparticles to the amine groups of 4-ABT on Pt (Ag@4-ABT/Pt), distinct Raman spectra were observed. Considering the fact that almost no Raman peaks are observed when Ag nanoparticles are attached to 4-aminophenylsilane monolayers assembled on a silicon wafer, the Raman spectra observed for Ag@4-ABT/Pt must be surface-enhanced Raman scattering (SERS) spectra, occurring through an electromagnetic (EM) coupling of the localized surface plasmon of Ag nanoparticles with the surface plasmon polariton of the Pt substrate. From the excitation wavelength dependence, we also confirmed the contribution of the charge-transfer enhancement in the SERS spectra of Ag@4-ABT/Pt: it became more important at short-wavelength excitation. Overall, the SERS intensity of Ag@4-ABT/Pt gradually decreased as the excitation wavelength was increased from 488 to 514.5, 568, and 632.8 nm. A similar trend was observed with a finite-difference time-domain calculation, suggesting that the EM coupling should also be strong at short-wavelength excitation. Accordingly, the experimental enhancement factor per Ag nanoparticle was estimated to be as large as 7.9×10^2 under the illumination of 514.5 nm radiation. The present observation clearly demonstrates that the inherent obstacles to the more widespread use of SERS can be overcome by the judicious use of SERS-active nanoparticles directly or indirectly.

1. Introduction

Noble metallic nanostructures exhibit a phenomenon known as surface-enhanced Raman scattering (SERS) in which the scattering cross sections are dramatically enhanced for molecules adsorbed thereon.[1,2] In recent years, it has been reported that even single-molecule spectroscopy is possible by SERS,[3−5] suggesting that the enhancement factor (EF) can reach as much as $10^{14}-10^{15}$. According to theoretical studies, at least 8−10 orders of magnitude can arise from electromagnetic surface plasmon excitation,[5,6] in addition to the chemical enhancement associated with either the metal-to-molecule or the molecule-to-metal charge-transfer transition. Lombardi and Birke[7] have shown recently that the SERS intensity can be expressed as a function of the product of three contributions, representing the surface plasmon resonance, the metal−molecule charge-transfer resonance at the Fermi energy, and an allowed molecular resonance. There is then a possibility that the charge-transfer contribution may dominate the SERS spectrum.

In agreement with the electromagnetic and chemical enhancement mechanisms, SERS is especially sensitive to the first layer of adsorbates. Accordingly, SERS has found important applications in many areas of chemistry, including chemical analysis, corrosion, lubrication, and heterogeneous catalysis.[8−12] However, SERS still has two specific obstacles.[2] One obstacle is that a large enhancement is limited to specifically two noble metals, Ag and Au, which severely limits wider applications involving other metallic materials of both fundamental and practical importance. The other obstacle is that, even for Ag and Au metals, a surface morphology with a roughness scale of 50−200 nm is crucial to exhibiting a large enhancement factor. In recent years, even transition metals have been proven to be SERS-active when they were subjected to proper roughening processes.[13−15] In any case, atomically flat surfaces, commonly used in the area of surface science and nanotechnology, are not suitable for SERS investigation.

To use SERS in routine, online studies for analytical purposes, SERS spectra should be obtainable even for the molecules anchored on solid surfaces with negligible SERS activity. One promising approach would be the introduction of so-called tip-enhanced Raman spectroscopy (TERS).[16] By illuminating the gap (with a width of 1 to several nm) between a silver or gold tip of a scanning probe microscope and a metal substrate with a laser of suitable wavelength, localized surface plasmons can be excited inside the gap, producing a large increase of the electromagnetic field and thus resulting in a significant increase in the Raman intensity in a region having the size of the tip apex.[17,18] An alternative way to mimic TERS would be the use of Ag or Au nanoparticles such that the gap between the metal nanoparticle and the planar metal substrate could function as a hot site for SERS. In fact, we and others have demonstrated recently that very intense SERS spectra could be obtained for 4-aminobenzenethiol (4-ABT) assembled on a macroscopically flat Ag or Au substrate simply by attaching Ag or Au nanoparticles to them.[19−22] On the basis of these observations, we have investigated in this work whether unaggregated Ag nanoparticles can also induce SERS for 4-ABT assembled on a macroscopically smooth Pt substrate (see Scheme 1). To the best of our knowledge, it is the first report that very intense SERS spectra can be obtained from adsorbates on Pt, intrinsically a weak SERS substrate, by assembling nanosized Ag

* To whom correspondence should be addressed. E-mail: kwankim@snu.ac.kr (K.K.), kshin@ssu.ac.kr (K.S.S.). Tel: +82-2-8806651 (K.K.), +82-2-8200436 (K.S.S.). Fax: +82-2-8891568 (K.K.), +82-2-8244383 (K.S.S.).

† Seoul National University.

‡ Soongsil University.

10.1021/jp105005a
Published on Web 07/23/2010

SCHEME 1: Schematic Diagram of a Nanogap, Formed by a Planar Pt(Au) Substrate and a Ag Nanoparticle, in Which a Probe Molecule, 4-Aminobenzenethiol, Is Bound via Thiolate Sulfur and an Amine Group to Pt(Au) and Ag, Respectively

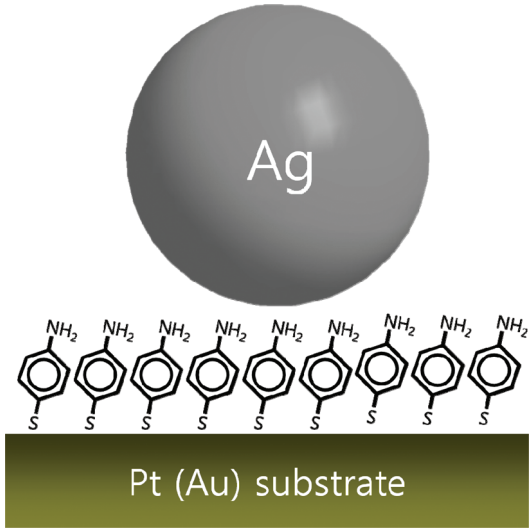

particles onto them. The dependence of EF values on the kind of base metal substrates, that is, Pt versus Au, is expected to provide valuable information regarding not only the optimum condition of TERS but also the nature of hot sites for SERS in general. The electromagnetic properties around a Ag nanoparticle−Pt plane junction, as well as a Ag nanoparticle−Au plane junction, were also modeled using the three-dimensional finite-difference time-domain (3D-FDTD) method,[23] and it turned out that more intense Raman spectra, and thus the greater EFs, should be measured on Pt at 488 nm excitation than at 632.8 nm excitation, but at 632.8 nm excitation than at 488 nm excitation on Au, which is in agreement with the actual observation.

2. Experimental Section

The chemicals otherwise specified were reagent grade, and ultrapure water, with a resistivity greater than 18.0 MΩ·cm (Millipore Milli-Q System), was used in making aqueous solutions. A Pt substrate (0.1 mm thick, 99.99%, Aldrich) was polished to a mirror finish using 0.05 μm alumina powder and then sonicated sequentially in isopropyl alcohol, hot piranha solution, and water. For a comparative study, a Au substrate (0.1 mm thick, 99.99%, Aldrich) was also polished and then washed similarly before use. The self-assembly of 4-ABT (97%, Aldrich) on Pt and Au substrates was conducted in 1 mM ethanolic solution for 12 h. For a control experiment, a 4-aminophenyl-derivatized silicon wafer was also prepared following the prorocol in the literature.[24]

Ag sol was prepared by following the recipes of Lee and Meisel.[25] Initially, an amount of 100 mL of silver nitrate solution containing 17 mg of $AgNO_3$ was brought to a boil. A solution of 1% sodium citrate (2 mL) was then added to the $AgNO_3$ solution under vigorous stirring, and boiling was continued for ~30 min. The Ag sol thus prepared was stable for several weeks, and the Ag nanoparticles were of a nearly spherical shape with an average diameter of ~62 nm (vide infra). To attach the Ag nanoparticles to the pendent NH_2 groups of 4-ABT on Pt or Au (denoted by Ag@4-ABT/Pt or Ag@4-ABT/Au, respectively), as well as onto the 4-aminophenyl groups on a silicon wafer (denoted by Ag@4-APS/Si), these substrates were soaked in Ag sol for 1 h. After washing with water and ethanol consecutively, the substrates were left to dry in a vacuum for 2 h and then subjected to Raman spectral analyses.

UV/vis spectra were obtained with a SCINCO S-4100 spectrometer. The ζ potential of the Ag nanoparticles was measured in a Malvern Zetasizer 3000HS (Malvern Instruments, U.K.). TEM images were acquired using a JEM-200CX transmission electron microscope at 160 kV. Field emission scanning electron microscopy (FE-SEM) images were obtained with a JSM-6700F field emission scanning electron microscope operating at 5.0 kV.

Raman spectra were obtained using a Renishaw Raman system model 2000 spectrometer equipped with an integral microscope (Olympus BH2-UMA). The 488 and 514.5 nm lines from a 20 mW Ar^+ laser (Melles-Griot model 351MA520), the 568 nm line from a 20 mW Ar^+/Kr^+ laser (Melles-Griot model 35KAP431), or the 632.8 nm line from a 17 mW He/Ne laser (Spectra Physics model 127) were used as the excitation source. Raman scattering was detected over 180° using a Peltier cooled (−70 °C) charge-coupled device (CCD) camera (400 × 600 pixels). The laser beam was focused onto a spot approximately 1 μm in diameter with an objective microscope with magnification of the order of 20×. The data acquisition time was usually 30 s. The holographic grating (1800 grooves/mm) and the slit allowed the spectral resolution to be 1 cm^{-1}. The Raman band of a silicon wafer at 520 cm^{-1} was used to calibrate the spectrometer, and the accuracy of the spectral measurement was estimated to be better than 1 cm^{-1}.

3D-FDTD electrodynamics simulation[23] was carried out with FDTD solutions software provided by Lumerical Solutions, Inc. A nanostructure composed of a silver nanoparticle and a flat platinum (or gold) surface was modeled as a single silver sphere (60 nm) laid on a cubical platinum (or gold) substrate with dimensions of 400 nm ×400 nm ×150 nm. The gap between the sphere and the cuboid was fixed to be 1 nm. The dielectric constants of the silver, gold, and platinum were taken from the source program. The propagation directions of plane waves (488, 514.5, 568, and 632.8 nm wavelength) were chosen to be along the x or z axis. In each case, the electric field was assumed to be polarized along the z axis and $y$axis, respectively. Boundary conditions were imposed by means of the perfectly matched layer method. After the computation of the local electric field, the field intensity was evaluated for each mesh by integration and finally compared with the EF values estimated from the measured Raman spectra.

3. Results and Discussion

As a probing adsorbate, 4-ABT is chosen on the grounds that the molecule is expected to adsorb very favorably not only onto Au but also onto Pt by forming a metal−thiolate bond such that Ag nanoparticles can adsorb subsequently onto the pendent amine group. It is well known that 4-ABT forms a close-packed monolayer on Au by forming Au−S bonds after deprotonation.[26] Rosario-Castro et al.[27] recently reported that 4-ABT also forms a close-packed monolayer on Pt by forming Pt−S bonds. On the other hand, the citrate-reduced Ag nanoparticles are negatively charged so that the particles can be bound to the positively charged amine groups via electrostatic attraction in a solution phase:[20,21] In ambient conditions, Ag nanoparticles will subsequently bind directly to the nitrogen lone pair electrons of the amine groups of 4-ABT.

At the beginning, we confirmed that no Raman peak is identifiable for 4-ABT assembled on a Pt substrate, irrespective

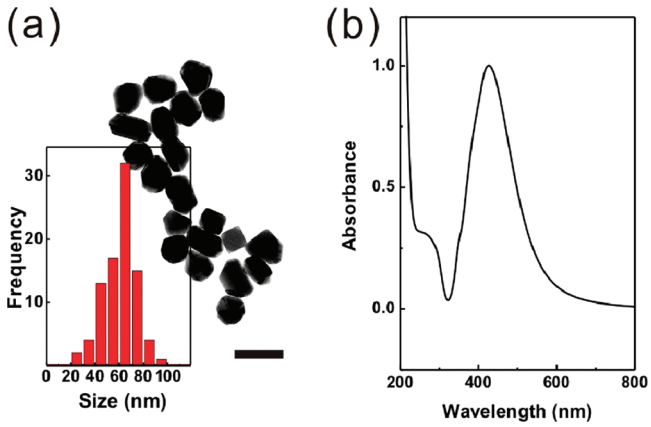

Figure 1. (a) Typical TEM image of Ag nanoparticles (scale bar = 100 nm). The inset shows a histogram of the particle size distribution. (b) UV/vis absorption spectrum of Ag citrate sol.

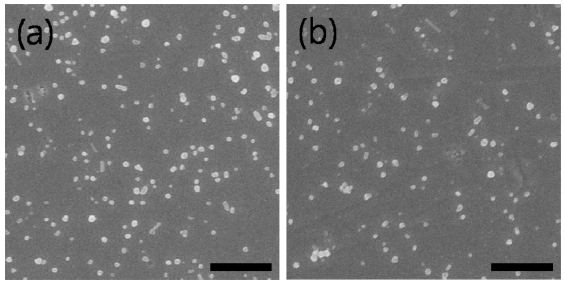

Figure 2. FE-SEM images of (a) Ag@4-ABT/Pt and (b) Ag@4-ABT/Au measured after soaking in Ag sol for 1 h (scale bar = 1 μm).

of the excitation wavelength in the region of 488−632.8 nm. As will be shown below, Raman peaks due to 4-ABT appeared, however, once the 4-ABT-adsorbed Pt substrate was soaked in Ag sol. This indicates, first, that 4-ABT adsorbs on Pt and, second, that Ag nanoparticles are bonded to the amine groups of 4-ABT on Pt. Because Ag nanoparticles are critically important in this respect, we first show in Figure 1a the TEM image of Ag sol particles prepared in this work. According to the histogram in the inset of Figure 1a, the mean diameter of Ag nanoparticles is determined to be 62 ± 15 nm (vide supra). As shown in Figure 1b, these Ag particles exhibited a very distinct surface plasmon absorption band at 425 nm: It is well separated from the Raman laser wavelengths used in this work. On the other hand, the ζ-potential measurement indicated that the Ag nanoparticles are negatively charged, that is, −25 mV, presumably due to the deprotonation of the citrate moiety.

To see how effectively those Ag nanoparticles could bind to the terminal amine group of 4-ABT on Pt, we conducted FE-SEM analysis and observed that the surface coverage of Ag nanoparticles was at most ~3%, even after soaking in Ag sol for 1 h. A similar distribution was observed in the FE-SEM image of Ag nanoparticles adsorbed on 4-ABT on a Au substrate. Those Ag nanoparticles were quite evenly distributed over the 4-ABT monolayers without coagulation in either case. This is evident from the FE-SEM images in Figure 2a,b, each of which were measured after soaking the 4-ABT/Pt and 4-ABT/Au substrates in Ag sol for 1 h, respectively. The surface coverage of Ag nanoparticles on 4-ABT/Pt is determined to be 8 particles/μm^2, while that on 4-ABT/Au is 6 particles/μm^2. Because the Ag nanoparticles were separated, on average, by 200 nm, no SERS peaks should be significantly affected by their mutual interaction. The subsequent experiment was thus conducted after soaking in Ag sol for 1 h.

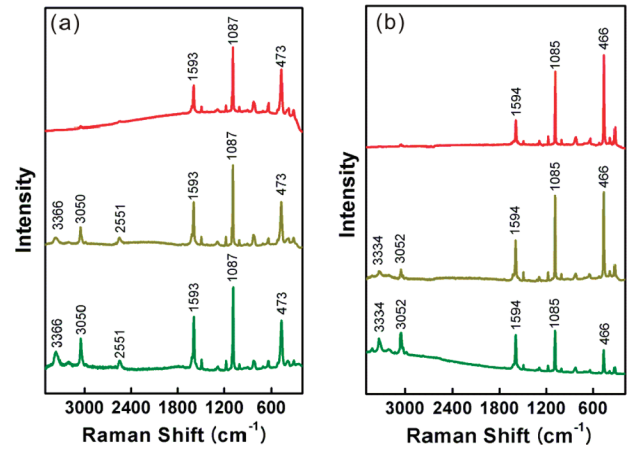

Figure 3. Normal Raman spectra of 4-ABT (a) in a neat solid state and (b) in an anionic state in alkaline solution, taken using the 632.8 nm line of a He/Ne laser (top), the 568 nm line of an Ar/Kr laser (middle), and the 514.5 nm line of an Ar ion laser (bottom) as excitation sources. All spectral intensities were normalized with respect to those of silicon wafers used for instrument calibration.

For a better interpretation of the SERS spectra, we obtained the normal Raman (NR) spectra of 4-ABT in its neat and anionic states using 514.5, 568, and 632.8 nm radiation as the excitation sources. The peak intensities, as well as the peak positions, at specific excitation wavelengths were all normalized with respect to the Raman band of a silicon wafer appearing at 520 cm^{-1}. The normalized Raman spectral patterns shown in Figure 3 are largely independent of the excitation wavelength. Any spectral difference between neat and anionic states is due to the deprotonation of the thiol in the anionic state. The major peaks in Figure 3 are collectively summarized in Table 1 along with their vibrational assignment.

Figure 4a,b shows the Raman spectra of Ag@4-ABT/Pt and Ag@4-ABT/Au, respectively, taken using 488, 514.5, 568, and 632.8 nm radiation as the excitation source. To minimize any effect due to inhomogeneous distribution of the Ag nanoparticles, we actually took the Raman spectra while spinning the sample at 3000 rpm. Although some excitation wavelength dependence is observed, it is remarkable that SERS spectra can be obtained even from a SERS-inactive metal substrate by virtue of Ag nanoparticles. Major peaks observed using a laser excitation of 568 nm are also listed in Table 1. It should be mentioned that only a featureless spectrum is obtained when Ag nanoparticles are attached onto 4-aminophenylsilane monolayers assembled on a silicon wafer (data not shown). This indicates that Ag nanoparticles adsorbed on amino groups are neither hot particles nor hot clusters to exhibit EM enhancement. In the absence of EM enhancement, any chemical enhancement will also be harder to identify. The appearance of Raman peaks in Figure 4a,b can then be attributed to the electromagnetic coupling of the localized surface plasmon of Ag nanoparticles with the surface plasmon polariton of the Pt or Au substrates.

It is noteworthy in Figure 4 that the SERS spectral pattern for Ag@4-ABT/Pt is comparable to that for Ag@4-ABT/Au. This would indicate that the SERS spectral feature was determined mainly by the Ag nanoparticles. Although the b_2-type bands (i.e., 9b at 1143, 3 at 1390, and 19b at 1435 cm^{-1}) are hardly observed in the NR spectra in Figure 3, those bands appeared distinctly in the SERS spectra of Ag@4-ABT/Pt and Ag@4-ABT/Au in Figure 4. The appearance of the b_2-type bands in the SERS spectra of 4-ABT adsorbed onto a Ag electrode was attributed by Osawa et al.[28] to the chemical (or charge-transfer) enhancement mechanism: The b_2-mode en-

TABLE 1: Raman Spectral Peaks of 4-Aminobenzenethiol Measured in Free and Surface Adsorbed States Using the Excitation Laser of 568 nm

normal Raman[a]		SERS[a]		
neat (solid)	anion state	Ag@4-ABT/Pt	Ag@4-ABT/Au	vibrational assignment[b]
	3422vw			
3366vw	3334vw			
3050vw	3052vw			νCH, 2(a_1)
	3031vw			νCH, 13(a_1)
	2990vw			
2551vw				νSH
1737vw	1737vw			
1616w	1627vw			δNH
1593 m	1594 m	1586 m	1592w	νCC, 8a(a_1)
1570vw	1568vw	1577 m	1585 m	νCC, 8b(b_2)
		1517vw		
1492vw	1495vw		1489w	νCC + δCH, 19a(a_1)
		1472vw	1475w	
1422vw	1423vw	1435 m	1437s	νCC + δCH, 19b(b_2)
1367vw	1371vw	1390 m	1390 m	νCC + δCH, 3(b_2)
			1311vw	νCC + δCH, 14(b_2)
1286w	1290vw			
			1233vw	
1176w	1180w	1178w	1186vw	δCH, 9a(a_1)
1150vw		1143 m	1145s	δCH, 9b(b_2)
1099w	1091w			
1087 m	1085 m	1076 m	1079 m	νCS, 7a(a_1)
1008vw	1008vw	1004w	1006vw	γCC + γCCC, 18a(a_1)
			920vw	πCH, 5b(b_1)
907vw				δSH
829w	828w			
		819vw	818vw	
713vw	714vw	717vw	714vw	πCH + πCS + πCC, 4b(b_1)
644w	649w	639vw	640vw	γCCC, 12(a_1)
		543vw	544vw	
519vw	524vw			γCCC, 16b(b_1)

[a] Unit in wavenumber (cm^{-1}). [b] Taken from ref 20 denoting ν, stretch; δ and γ, bend; π, wagging; τ, torsion; vs, very strong; s, strong; m, medium; w, weak; and vw, very weak. The ring modes correspond to those of benzene under C_{2v} symmetry.

hancement was interpreted in terms of the Herzberg−Teller (vibronic) coupling terms.[7] Recently, Zhou et al.[29] proposed that the enhancement of SERS spectra of 4-ABT trapped in a gap site of a Au substrate and Ag nanoparticles is due to charge tunneling enhancement. A similar charge tunneling would also occur from the Ag nanoparticles to the Pt or Au substrates in our sandwich structures.

The involvement of the charge-transfer (CT) enhancement mechanism would be confirmed from the excitation wavelength dependence of the relative peak intensity of the b_2 mode to the a_1 mode.[7] In this respect, we have evaluated the band areas of the two strong b_2 bands (3 and 19b), as well as that of one strong a_1 band (7a) in all spectra in Figure 4. Figure 5a,b shows the peak intensity of these a_1 and b_2 bands, as well as their relative intensity (b_2-to-a_1), drawn versus the excitation laser wavelength, measured for Ag@4-ABT/Pt and Ag@4-ABT/Au, respectively. For Ag@4-ABT/Pt, both the a_1 and the b_2 bands are seen to increase in intensity as the excitation wavelength is decreased from 632.8 to 488 nm, while the same bands decrease in intensity for Ag@4-ABT/Au. Considering that the a_1-type band is usually assumed to be enhanced via an EM mechanism,[20,28] this would suggest that the EM coupling between the Ag nanoparticle and the Pt substrate is more efficient in the

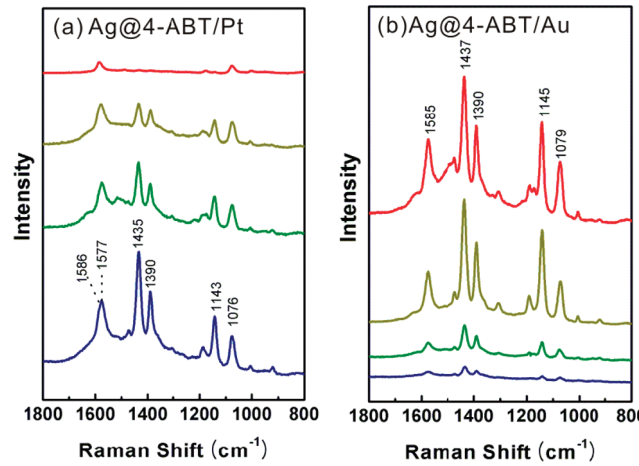

Figure 4. SERS spectra of 4-ABT on flat (a) Pt and (b) Au taken after soaking in Ag sol using the 632.8, 568, 514.5, and 488 nm radiation (from top to bottom) as the excitation sources. All spectra were taken while spinning at 3000 rpm to minimize the effect of the inhomogeneous distribution of Ag nanoparticles. In addition, all spectral intensities were normalized with respect to those of silicon wafers used for instrument calibration and also to the number of Ag nanoparticles adsorbed on 4-ABT on Pt or Au.

short-wavelength region, although the EM coupling between the Ag nanoparticle and the Au substrate is more efficient in the long-wavelength region. In either case, however, the 3 and 19b bands (b_2) are seen to decrease with respect to the 7a band (a_1) as the excitation wavelength is increased. This clearly indicates that the chemical enhancement mechanism is involved in all Raman spectra in Figure 4.

As mentioned previously, a Ag nanoparticle itself is not "hot" enough to induce SERS via EM and CT mechanisms. Hence, the SERS spectra in Figure 4 must have been the result of the product of the surface plasmon resonance, associated with the EM coupling of Ag nanoparticles and the planar Pt or Au substrates, and the metal−molecule CT resonance at the Fermi energy. For both Ag@4-ABT/Pt and Ag@4-ABT/Au systems, the degree of CT must decrease as the excitation wavelength is increased. Anyhow, a close look at Figure 5 reveals that the relative peak intensities of b_2 bands (3 and 19b) normalized with respect to that of the a_1 band (7a) are larger in Ag@4-ABT/Au than in Ag@4-ABT/Pt in all excitation wavelengths. This may reflect the difference in the Fermi energy of Au (5.0 eV)[30] and Pt (5.9 eV):[31] The Fermi energy of Ag is 4.3 eV.[31] Figure 6 shows the Fermi levels of Ag, Au, and Pt from the vacuum, along with the π and π^* levels of 4-ABT: The ionization potential of 4-ABT is 7.16 eV (which locates the filled π orbital), and its lowest unfilled π^* orbital (LUMO) is located at 3.03 eV from the vacuum.[32] The energy gaps between the Ag, Au, and Pt Fermi levels and the π^* molecular level of 4-ABT are 1.27, 1.97, and 2.87 eV, respectively, whereas the energy gaps between the same Fermi levels and the π molecular level are 2.86, 2.16, and 1.26 eV, respectively. The photon energies of a laser with $\lambda = 488$, 514.5, 568, and 632.8 nm are calculated to be 2.54, 2.41, 2.18, and 1.96 eV, respectively, so that based on the energy matching conditions, a CT transition, either from the metal to the π^* orbital of 4-ABT or from the π orbital of 4-ABT to the metal, can be more facile using a shorter wavelength laser, as actually observed. It seems also not unreasonable to suppose that a CT transition is less likely in Ag@4-ABT/Pt than in Ag@4-ABT/Au in all excitation wavelengths (from 488 to 632.8 nm).

We have estimated the effective EFs per Ag nanoparticle for the Ag@4-ABT/Au and Ag@4-ABT/Pt systems. For that

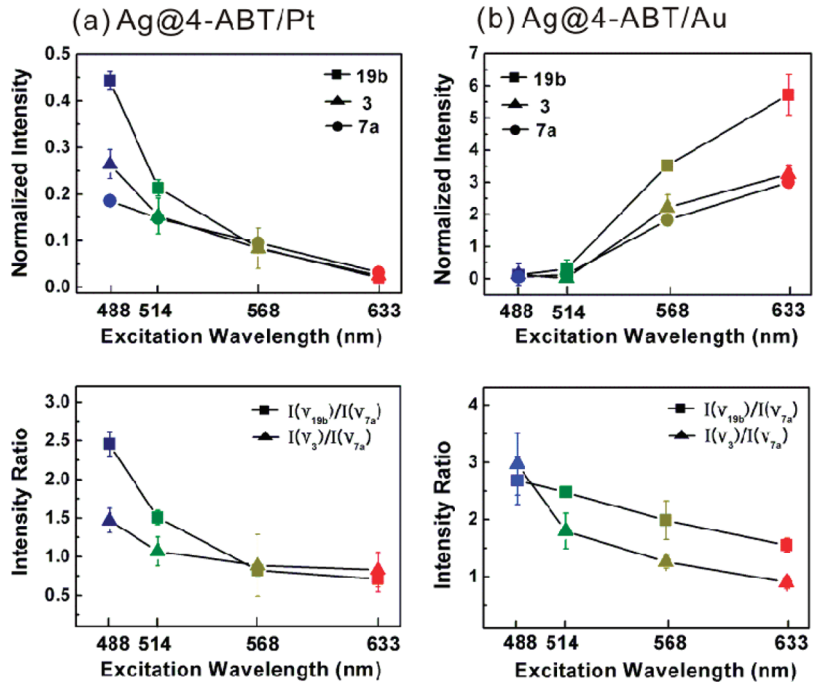

Figure 5. (top panels) Peak intensities of 19b, 3, and 7a bands of 4-ABT normalized with respect to the Raman band of a silicon wafer at 520 cm^{-1} and (bottom panels) their ratios with respect to that of the 7a band, that is, $I(\nu_{19b})/I(\nu_{7a})$ and $I(\nu_3)/I(\nu_{7a})$, drawn versus excitation wavelength in Raman spectra of (a) Ag@4-ABT/Pt and (b) Ag@4-ABT/Au shown in Figure 4. All of the symbols shown were the average of five different measurements with the error bars denoting their standard deviation.

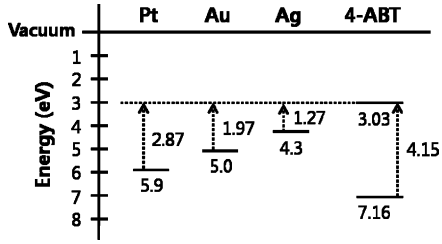

Figure 6. Fermi levels of Pt, Au, and Ag and molecular orbitals of 4-ABT.

purpose, we compared the SERS and NR intensities of the 7a band of 4-ABT at ~1080 cm^{-1} in Figure 4. Initially, the number of 4-ABT molecules illuminated by the laser light used in obtaining the NR spectra in Figure 3 was estimated by taking account of the facts that the size of the laser spot is ~1 μm, its penetration depth into 4-ABT is ~40 μm,[21] and the density of 4-ABT in the solid state is 1.18 g/cm^3.[33] Assuming that the sampling volume is well represented by the product of the laser spot size and its penetration depth, the number of 4-ABT molecules illuminated is calculated to be 1.8×10^{11} (i.e., 3.0×10^{-13} mol). We subsequently estimated the number of 4-ABT molecules that could be present on the planar Au and Pt substrates. Invoking the fact that each 4-ABT molecule occupies an area of ~0.20 nm^2 at the full coverage limit on Au,[34] the number of 4-ABT molecules that can be illuminated by a 1 μm sized laser beam is calculated to be 3.9×10^6 (i.e., 6.5×10^{-18} mol): in this estimation, we ignore the surface roughness of the Au substrate. We further assume that the surface coverage of 4-ABT on Pt is comparable to that on Au. The ratio of the numbers of 4-ABT molecules illuminated in NR and SERS spectral measurements would then amount to 4.6×10^4 (i.e., $1.8 \times 10^{11}/3.9 \times 10^6$). The apparent EF values may then be obtained by dividing the latter value with the intensity ratio of the 7a band of 4-ABT in NR and SERS spectra. Dividing further the apparent EF values with the averaged number of Ag nanoparticles/μm^2 on 4-ABT on a planar Au and Pt should result in EF values per Ag nanoparticle for the Ag@4-ABT/Au and Ag@4-ABT/Pt systems, respectively.

In this way, the EFs per Ag nanoparticle for Ag@4-ABT/Au are estimated to be 7.0×10^2 and 1.7×10^4 for the 514.5 and 632.8 nm excitation, respectively. We noticed that the EF value (i.e., 1.7×10^4) obtained herein for the 632.8 nm excitation is comparable to that estimated in our previous report (i.e., 9.2×10^3).[20] On the other hand, the EFs per Ag nanoparticle for Ag@4-ABT/Pt are estimated to be 7.9×10^2 and 2.0×10^2 for the 514.5 and 632.8 nm excitation, respectively. The present observation suggests that the Ag nanoparticle-to-Pt interaction is more favorable for SERS induction than the Ag nanoparticle-to-Au interaction, at least under the illumination of short-wavelength light. This implies that the surface plasmon frequency of Ag nanoparticles can be coupled more efficiently to the surface plasmon polariton of the Pt substrate rather than to that of the Au substrate. As the wavelength of the laser light is increased, for instance, from 514.5 to 632.8 nm, the laser light can resonate more easily with the surface plasmon polariton of the Au substrate than that of the Pt substrate. The SERS signal of 4-ABT in Ag@4-ABT/Au will then be observed to increase in the order of 488 < 514.5 < 568 < 632.8 nm excitation, while the SERS signal in Ag@4-ABT/Pt shows the opposite trend. Anyhow, the overridden Ag nanoparticles must play an important role in the induction of SERS via electromagnetic coupling with the underneath Pt or Au substrate.

To rationalize the experimental observation, we have carried out 3D-FDTD simulations. The FDTD method is an explicit time-marching algorithm used to solve Maxwell's curl equations on a discrete spatial grid. It can be used for studying both the near and the far field electromagnetic responses for heterogeneous materials of arbitrary geometry.[35] As described in the Experimental Section, in this simulation, a nanostructure was modeled to be composed of a single silver sphere of 60 nm in

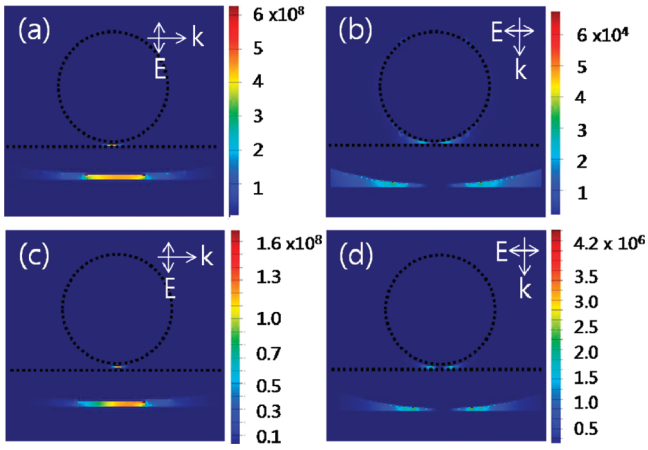

Figure 7. Intensity distribution ($|E/E_0|^4$) of the induced local electric field E relative to the excitation field E_0 near a Ag sphere (60 nm) and (a, b) Pt and (c, d) Au cuboids, calculated by the 3D-FDTD method in a condition that the electric field (514.5 nm radiation) is directed perpendicular (a, c) or parallel (b, d) to the surface of the Pt or Au cuboid. Insets are the magnified images of the gap sites.

diameter laid on a cubical platinum (or gold) substrate with dimensions of 400 nm ×400 nm ×150 nm. The gap distance between the Ag sphere and Pt (or Au) cuboid was fixed to be 1 nm. Figure 7 shows the 3D-FDTD results calculated under the illumination of 514.5 nm radiation. It can be seen that the intensity of the induced electric field is extremely sensitive to the polarization direction of the incident radiation. As one may expect, only a single maximum is located exactly at the gap in a perpendicular polarization, whereas two maxima are present in a parallel polarization in Figure 7. In the latter case, the center of the gap is a node. In either case, because the "hot" site is highly localized, most of the SERS signal must arise from a small area of the junction.

In the 3D-FDTD calculation, both the incident light field and the Raman scattered field were clearly seen to increase. Because the Raman scattering enhancement scales roughly as $|E/E_0|^4$ (E and E_0 are the local and input fields, respectively),[36] an extremely large SERS enhancement will be possible with only a modest electromagnetic field augmentation. In fact, in cases when the incident light was polarized along a normal (out-of-plane) direction to the Pt surface, the maximum EF value, $EF_{max} = |E_{max}/E_0|^4$, was computed to be 1.75×10^4 at the 514.5 nm excitation, whereas the maximum EF value under a parallel (in-plane) light was at best 4.61. A much stronger enhancement must then occur using a perpendicularly polarized light. On the Au surface, the corresponding EF values were computed to be 2.99×10^3 and 1.42×10^1, respectively. It is astonishing that the EF value from Ag@4-ABT/Pt is an order of magnitude greater than that from Ag@4-ABT/Au, at least under the illumination of 514.5 nm radiation. As can be seen in Figure 4, the most intense Raman peaks were, in fact, observed from Ag@4-ABT/Pt than Ag@4-ABT/Au when the 514.5 nm radiation was used as the excitation source.

In Figure 8, the simulated EF values (as a function of the excitation wavelength) are shown together with the experimental ones. The experimentally determined EF values are obviously greater than the 3D-FDTD result obtained in a parallel polarization, but mostly smaller than that computed in a perpendicular polarization. To facilitate a better comparison with the theoretical results, it should be remembered that, in our experimental configuration, the laser beam was directed along the normal to the sample. In this configuration, the incident light would be considered mostly to be polarized parallel to the substrate.

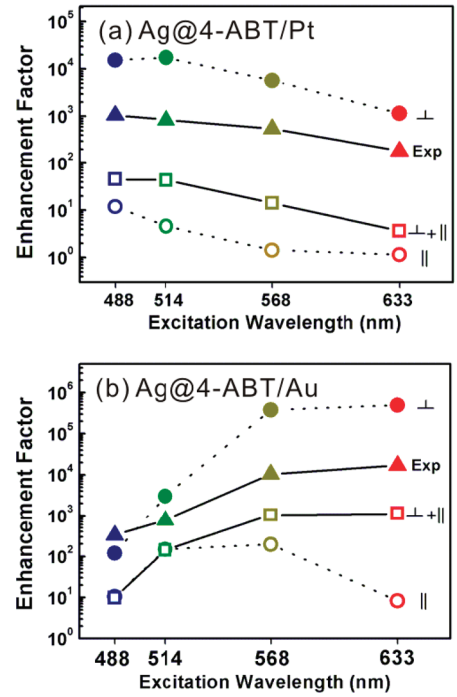

Figure 8. Experimental and theoretical enhancement factors (EFs) determined for the 7a band of 4-ABT in (a) Ag@4-ABT/Pt and (b) Ag@4-ABT/Au drawn versus the excitation wavelengths. (filled triangles, exp) Experimental EFs determined by referring to the SERS spectra shown in Figure 4. (filled circles, ⊥) Theoretical EFs predicted using the 3D-FDTD method under conditions in which the electric field is directed perpendicular to the planar Pt or Au. (open circles, ||) Theoretical EFs when the applied electric field is parallel to the planar Pt or Au. (open squares, ⊥ + ||) Theoretical EFs computed by taking into account the portions of the perpendicular and parallel polarizations in an actual experimental condition.

However, we have to acknowledge that a lens with a very short focal length is used to measure the Raman spectra. A part of the laser beam will be highly refracted, especially at the edge in this case. A perpendicularly polarized beam will then inevitably be present at the sampling position. In this sense, we have accordingly estimated the percentage of a perpendicularly polarized beam taking into consideration the fact that the diameter of the laser beam used is 7 mm (before focusing) and the focal length of the object lens is 9 mm. To mimic the experimental EF values better, we have thus computed new theoretical EF values by weighting the contribution of perpendicular and parallel polarized light, and the result is also represented in Figure 8. The simulations performed this way confirm the experimental observations more qualitatively. It is evident that the EF value for Ag@4-ABT/Pt increases as laser light with a shorter wavelength in the order of 488 > 514.5 > 568 > 632.8 nm is used as the excitation source, whereas the EF value for Ag@4-ABT/Au decreases in that case. As mentioned previously, this may reflect the fact that a more favorable electromagnetic coupling is possible when the wavelength of the illuminating light is closer to both the localized surface plasmon resonance wavelength of Ag nanoparticles and the surface plasmon polariton wavelength of planar Pt or Au. This also suggests that the efficiency of TERS will be greatly dependent on the kind of metallic substrate.

4. Summary and Conclusion

Platinum is intrinsically a weak SERS substrate, but we have confirmed in this work that very intense SERS spectra can be

obtained from adsorbates on Pt by assembling nanosized Ag particles onto them. Specifically, we have compared the SERS intensity of 4-ABT in Ag@4-ABT/Pt with that in Ag@4-ABT/Au and found that the more intense spectra are measured in the former at least under the illumination of a short-wavelength laser, that is, 488 and 514.5 nm. This spectral enhancement must be ascribed to a more facile electromagnetic coupling of the silver particle and the platinum substrate in short-wavelength regions. That is, the localized surface plasmon of the silver particle must interact more favorably with the surface plasmon polariton of the Pt substrate in the short-wavelength regions. For Ag@4-ABT/Au, however, a very intense spectrum of 4-ABT was observed using a long-wavelength laser, that is, 632.8 nm, reflecting that the electromagnetic coupling of the silver particle with Au should be stronger comparatively in the long-wavelength regions. These wavelength-dependent behaviors were found also to agree with the 3D-FDTD calculations. In addition to the EM enhancement, we also confirmed the contribution of the CT enhancement. In both Ag@4-ABT/Pt and Ag@4-ABT/Au, the CT was more favorable in the shorter excitation wavelength region. In the longer excitation wavelength region, the CT appeared to be more facile in Ag@4-ABT/Au than in Ag@4-ABT/Pt. These could be understood in terms of the difference in the Fermi energy of Pt and Au. The implication of the present observation is enormous because it strongly suggests that the inherent obstacles to the more widespread use of SERS can be overcome by the judicious use of SERS-active nanoparticles directly or indirectly.

Acknowledgment. This work was supported by the National Research Foundation of Korea Grant funded by the Korean Government (Grant Nos. 2010-0001637, M10703001067-08M0300-06711-Nano2007-02943, KRF-2008-313-C00390, and 2009-0072467).

References and Notes

(1) Chang, R. K.; Furtak, T. E. *Surface Enhanced Raman Scattering*; Plenum Press: New York, 1982.
(2) Moskovits, M. *Rev. Mod. Phys.* **1985**, *57*, 783.
(3) Nie, S.; Emory, S. R. *Science* **1997**, *275*, 1102.
(4) Xu, H.; Bjerneld, E. J.; Käll, M.; Börjesson, L. *Phys. Rev. Lett.* **1999**, *83*, 4357.
(5) Futamata, M.; Maruyama, Y.; Ishikawa, M. *Vib. Spectrosc.* **2002**, *30*, 17.
(6) Jiang, J.; Bosnick, K.; Maillard, M.; Brus, L. *J. Phys. Chem. B* **2003**, *107*, 9964.
(7) Lombardi, J. R.; Birke, R. L. *J. Phys. Chem. C* **2008**, *112*, 5605.
(8) Ni, J.; Lipert, R. J.; Dawson, G. B.; Porter, M. D. *Anal. Chem.* **1999**, *71*, 4903.
(9) Kim, N. H.; Lee, S. J.; Kim, K. *Chem. Commun.* **2003**, 724.
(10) Cao, P.; Gu, R.; Tian, Z. Q. *Langmuir* **2002**, *18*, 7609.
(11) Chu, W.; LeBlanc, R. J.; Williams, C. T.; Kubota, J.; Zaera, F. *J. Phys. Chem. B* **2003**, *107*, 14365.
(12) Tian, Z. Q.; Ren, B.; Wu, D. Y. *J. Phys. Chem. B* **2002**, *106*, 9463.
(13) Tian, Z. Q.; Ren, B.; Mao, B. W. *J. Phys. Chem. B* **1997**, *101*, 1338.
(14) Ren, B.; Li, X. Q.; She, C. X.; Wu, D. Y.; Tian, Z. Q. *Electrochim. Acta* **2000**, *46*, 193.
(15) Huang, Q. J.; Lin, X. F.; Yang, Z. L.; Hu, J. W.; Tian, Z. Q. *J. Electroanal. Chem.* **2004**, *563*, 121.
(16) Bailo, E.; Deckert, V. *Chem. Soc. Rev.* **2008**, *37*, 921.
(17) Wessel, J. *J. Opt. Soc. Am. B* **1985**, *2*, 1538.
(18) Notingher, I.; Elfick, A. *J. Phys. Chem. B* **2005**, *109*, 15699.
(19) Zheng, J.; Zhou, Y.; Li, X.; Ji, Y.; Lu, T.; Gu, R. *Langmuir* **2003**, *19*, 632.
(20) Kim, K.; Yoon, J. K. *J. Phys. Chem. B* **2005**, *109*, 20731.
(21) Yoon, J. K.; Kim, K.; Shin, K. S. *J. Phys. Chem. C* **2009**, *113*, 1769.
(22) Uetsuki, K.; Verma, P.; Yano, T.; Saito, Y.; Ichimura, T.; Kawata, S. *J. Phys. Chem. C* **2010**, *114*, 7515.
(23) Sullivan, D. M. *Electromagnetic Simulation Using the FDTD Method*; IEEE Press: New York, 2000.
(24) Kim, K.; Lee, H. S. *J. Phys. Chem. B* **2005**, *109*, 18929.
(25) Lee, P. C.; Meisel, D. *J. Phys. Chem.* **1982**, *86*, 3319.
(26) Ulman, A. *Chem. Rev.* **1996**, *96*, 1533.
(27) Rosario-Castro, B. I.; Fachini, E. R.; Hernández, J.; Pérez-Davis, M. E.; Cabrera, C. R. *Langmuir* **2006**, *22*, 6102.
(28) Osawa, M.; Matsuda, N.; Yoshii, K.; Uchida, I. *J. Phys. Chem.* **1994**, *98*, 12702.
(29) Zhou, Q.; Li, X.; Fan, Q.; Zhang, X.; Zheng, J. *Angew. Chem., Int. Ed.* **2006**, *45*, 3970.
(30) Hill, I. G.; Schwartz, J.; Kahn, A. *Org. Electron.* **2000**, *1*, 5.
(31) Lide, D. R., Ed. *CRC Handbook of Chemistry and Physics*; CRC Press: Boca Raton, FL, 1998.
(32) Larsen, A. G.; Holm, A. H.; Roberson, M.; Daasbjerg, K. *J. Am. Chem. Soc.* **2001**, *123*, 1723.
(33) http://www.chemicalland21.com/lifescience/phar/4-AMINOTHIOPHENOL.htm.
(34) Gole, A.; Sainkar, S. R.; Sastry, M. *Chem. Mater.* **2000**, *12*, 1234.
(35) Oubre, C.; Nordlander, P. *J. Phys. Chem. B* **2004**, *108*, 17740.
(36) Kneipp, K.; Kneipp, H.; Itzkan, I.; Dasari, R. R.; Feld, M. S. *Chem. Rev.* **1999**, *99*, 2957.

JP105005A